Synchronizing Moore and Spiegel

N. J. Balmforth and R. V. Craster
Department of Theoretical Mechanics, University of Nottingham, Nottingham, NG7 2RD, United Kingdom

(Received 22 August 1997; accepted for publication 12 September 1997)

This paper presents a study of bifurcations and synchronization {in the sense of Pecora and Carroll [Phys. Rev. Lett. **64**, 821–824 (1990)]} in the Moore–Spiegel oscillator equations. Complicated patterns of period-doubling, saddle-node, and homoclinic bifurcations are found and analyzed. Synchronization is demonstrated by numerical experiment, periodic orbit expansion, and by using coordinate transformations. Synchronization via the resetting of a coordinate after a fixed interval is also successful in some cases. The Moore–Spiegel system is one of a general class of dynamical systems and synchronization is considered in this more general context. © *1997 American Institute of Physics.* [S1054-1500(97)02604-9]

Two (or more) dynamical systems can, under certain circumstances, be made to synchronize. That is, all the systems converge to the same temporal behavior even when the underlying dynamics are chaotic. This is not guaranteed to occur for all couplings, and even when it occurs it may cease if some system parameters are varied slightly. Therefore, methods by which this convergence can be achieved have recently been of much interest. Apart from an intrinsic interest in synchronization, there are also applications to a wide variety of subjects; these include cryptography, neural networks, electrical circuits, and coupled lasers. This paper explores the behavior of a relatively unstudied nonlinear oscillator, and its synchronization properties. The study is placed in a more general setting, which casts light upon the general synchronization properties of a wide class of dynamical systems.

I. INTRODUCTION

A. Master-slave synchronization

Synchronization is the term given to the phenomenon in which coupled nonlinear systems ultimately converge to the same temporal behavior after initial separation. The problem of synchronization for general forms of coupling has a wide ranging significance, but here we will be concerned with a special class of synchronizing systems. These are ''master-slave'' systems which are defined as follows.[1,2] Take two identical copies of a nonlinear system; for example, for a three-dimensional dynamical system,

$$\begin{pmatrix}\dot{x}\\ \dot{y}\\ \dot{z}\end{pmatrix}=\begin{pmatrix}f(x,y,z)\\ g(x,y,z)\\ h(x,y,z)\end{pmatrix}\quad\text{and}\quad\begin{pmatrix}\dot{X}\\ \dot{Y}\\ \dot{Z}\end{pmatrix}=\begin{pmatrix}f(X,Y,Z)\\ g(X,Y,Z)\\ h(X,Y,Z)\end{pmatrix},\tag{1}$$

where (x,y,z) and (X,Y,Z) are the coordinates of the phase spaces of the two systems and f, g, and h are prescribed functions. Then, select one system, (x,y,z), as the master and the other, (X,Y,Z), as the slave. We then couple the two systems by completely replacing a coordinate of the slave system by the corresponding coordinate of the master, discarding the redundant equation for the replaced variable. That is, if (for example) we select x as the ''synchronizing coordinate,'' or ''drive variable,'' then

$$\begin{pmatrix}\dot{x}\\ \dot{y}\\ \dot{z}\end{pmatrix}=\begin{pmatrix}f(x,y,z)\\ g(x,y,z)\\ h(x,y,z)\end{pmatrix}\quad\text{and}\quad\begin{pmatrix}\dot{Y}\\ \dot{Z}\end{pmatrix}=\begin{pmatrix}g(x,Y,Z)\\ h(x,Y,Z)\end{pmatrix}.\tag{2}$$

Finally, if $Y-y\to 0$ and $Z-z\to 0$ as $t\to\infty$, then we may say that the slave synchronizes to the master. Later, we consider another, related form of master-slave synchronization, but for now we work with the relationship between (1) and (2) as the operational definition of master-slave coupling.

Given the extreme sensitivity of a chaotic nonlinear system to its initial condition, synchronization is, at least initially, a surprising observation. However, the key point is that the slaved system in (2) is mathematically different from the original in (1) on a fundamental level. In fact, master-slave synchronization can be rigorously demonstrated for a number of dynamical systems, notably the Lorenz equations.[3] However, synchronization is not necessarily a property of general dynamical systems. Moreover, the phenomenon does not automatically occur for all drive variables, nor for all parameter values and initial conditions.

B. The Moore–Spiegel oscillator

The heart of this paper is a discussion of synchronization in the Moore–Spiegel system.[4] This system can be written in the forms,

$$\dot{x}=y,\quad \dot{y}=z,\tag{3}$$

$$\dot{z}=-z-(T-R+Rx^2)y-Tx,\tag{4}$$

or

$$\dddot{x}+\ddot{x}+(T-R+Rx^2)\dot{x}+Tx=0,\tag{5}$$

where R and T are constants. Solutions to these equations are thought to be chaotic (Refs. 4, 5, and 6; see Fig. 1).

 1054-1500/97/7(4)/738/15/$10.00

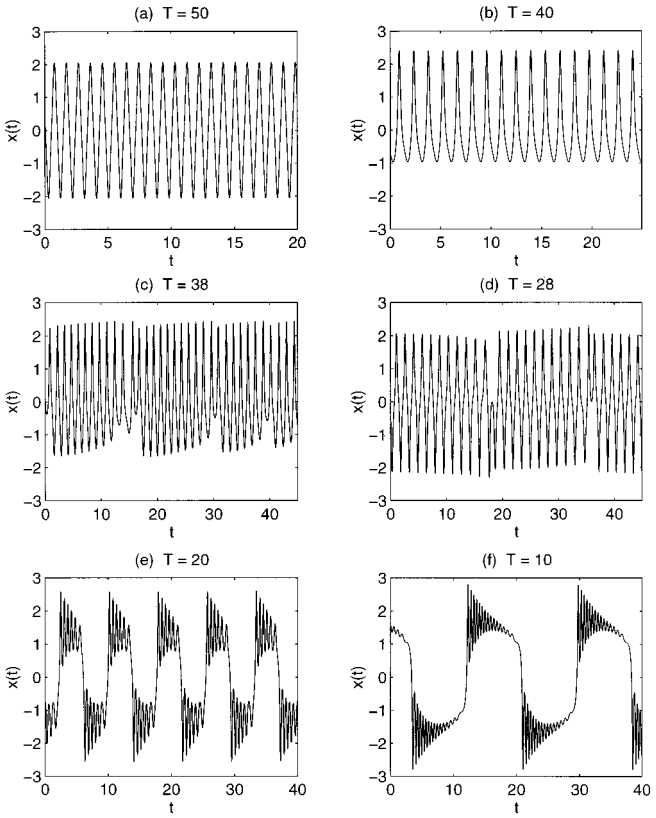

FIG. 1. Sample time series, $x(t)$, for $R=100$ and (a) $T=50$, (b) $T=40$, (c) $T=38$, (d) $T=28$, (e) $T=20$, and (f) $T=10$. The series in (a), (b), and (f) are periodic; those in (c), (d), and (e) appear to be chaotic. On average, (a), (d), (e), and (f) are symmetrical ($x\to -x$), but (b) and (c) are not.

The physical background to the model is in fluid mechanics. In essence, the model describes a small fluid element oscillating vertically in a temperature gradient with a linear restoring force. The element exchanges heat with the surrounding fluid and its buoyancy depends upon temperature. In other words, the system is a nonlinear thermomechanical oscillator with displacement $x(t)$. The parameter R corresponds to the Rayleigh number and T to the tension constant that quantifies the restoring force. Further details of the model can be found in Refs. 4 and 5.

In many senses it is, along with the Lorenz system, one of the classical low-order dynamical systems exhibiting chaos. However, in contrast to other nonlinear systems such as the Lorenz and Rössler equations, it has received less serious attention. This motivates us to give more than a cursory examination of the system itself in Sec. II.

Although both the Lorenz system and the Moore–Spiegel oscillator arise in the context of thermal convection, there are fundamental differences between the two systems. One of these differences lies in the form of the equations when parameters are set such that the systems are conservative.[6] For Moore–Spiegel, this limit is obtained when $R\to\infty$ and $T\to\infty$ with T/R order one. In fact, it is instructive to place both systems in a more general context, based upon their conservative forms. This proves valuable for considering synchronization properties of entire classes of dynamical systems.

C. Generalized potential systems

The conservative limit of Moore–Spiegel is obtained on making certain parameters diverge. Consequently, it is convenient to first rescale such that $\hat{t}=R^{1/2}t$, $\hat{x}=\delta^{-1/2}x$, $\delta=1-T/R$.[5] The Moore–Spiegel equations are then written in the form

$$\dot{x}=y,\quad \dot{y}=z,\quad \dot{z}=\delta(1-x^2)y-R^{-1/2}[z+(1-\delta)x], \tag{6}$$

on dropping the ''hat'' decoration. We then define the variable, λ, to replace z:

$$z=-\delta\lambda-\delta x\left(\frac{1}{3}x^2-1\right). \tag{7}$$

Thus the system becomes

$$\dot{x}=y,\quad \dot{y}=-\delta\lambda-\delta x\left(\frac{1}{3}x^2-1\right) \tag{8}$$

and

$$\dot{\lambda}=\frac{1}{\delta}R^{-1/2}\left(x-\frac{1}{3}\delta x^3-\delta\lambda\right). \tag{9}$$

The limit $R\to\infty$ is now straightforward.

This equivalent system allows an interpretation in terms of the motion of a particle in a time-varying potential $V(x,\lambda)$, where

$$V(x,\lambda)=\frac{x^4}{12}-\frac{x^2}{2}+\lambda x. \tag{10}$$

Then

$$\ddot{x}=-\delta\frac{\partial V}{\partial x}. \tag{11}$$

The equations can now be written as an example of a general class of potential systems that also includes the Lorenz and Rössler systems as particular cases. We define the class through the equations,

$$\dot{x}=y,\quad \dot{y}=-\frac{\partial V(x,\lambda)}{\partial x}-\nu y,\quad \dot{\lambda}=-\epsilon[\lambda+g(x)], \tag{12}$$

where ν and ϵ are positive constants, and $g(x)$ is a polynomial in x. The potential $V(x,\lambda)$ is

$$V(x,\lambda)=\frac{x^m}{m}-\sum_{k=1}^{m-1}\alpha_k(\lambda)\frac{x^k}{k} \tag{13}$$

with m an integer; for the Lorenz and Moore–Spiegel systems $m=4$ and for the Rössler system $m=3$, with various choices for the functions, $\alpha_k(\lambda)$, and the other parameters. Synchronization for this general class in investigated in Sec. V.

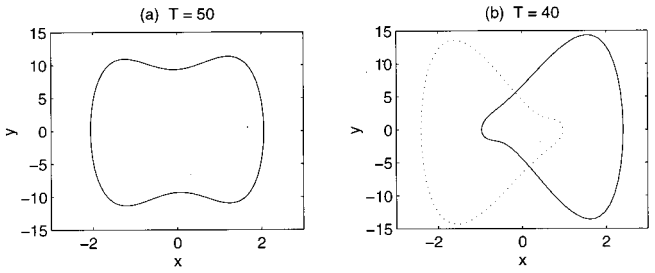

FIG. 2. (a) Symmetrical and (b) asymmetrical orbits projected onto the (x,y) plane.

II. THE MASTER SYSTEM

A. Preliminaries

The nonlinear system (3) and (4) has a fixed point at the origin. Provided $T>0$ and $R>0$ (the parameter regime of interest), this fixed point is always unstable. Instead, the system displays a perplexing array of periodic and aperiodic behavior (see Fig. 1). Shortly, we make sense of this zoology by constructing a bifurcation sequence obtained on varying T at fixed $R=100$ (we use this parameter value throughout this study). First, though, we make some preliminary remarks.

The Moore–Spiegel equations are invariant under the symmetry, $(x,y,z)\rightarrow(-x,-y,-z)$. Thus given one solution, we may always find another on applying the symmetry operation. Certain of the solutions shown in Fig. 1 also possess the symmetry, and so no new solutions are generated this way. Other solutions in Fig. 1, however, are asymmetrical and there are ''mirror'' copies of these objects.

Solutions to Eqs. (3) and (4) define orbits in the phase space (x,y,z). The orbits of the dynamical system describe a flow, $\mathbf{u}=(\dot{x},\dot{y},\dot{z})$, in this phase space. Importantly, the divergence of this velocity field is -1 for (3) and (4), or $-R^{-1/2}$ for (8) and (9). This indicates that the system is dissipative, and a finite initial volume of the flow will ultimately condense into a region with zero volume. That is, the system converges to an attractor with dimension less than three. We will visualize these attractors by phase portraits projected onto the (x,y) plane, and with Poincaré sections.

B. A bifurcation sequence

We begin at large T, since this is where the system has the simplest attractors: for $T>43.4$, the oscillator settles into a symmetrical limit cycle [Fig. 2(a)]. At $T\approx43.4$, the symmetrical limit cycle loses stability in a symmetry-breaking bifurcation (a necessary precursor to more complicated dynamics). This leads to a pair of asymmetrical limit cycles for smaller T [Fig. 2(b)]. These asymmetrical cycles persist stably down to $T\approx39.45$ where there is a period doubling bifurcation, followed by further ones at (slightly) smaller T (Fig. 3). This is the beginning of a cascade that leads to the object shown in Figs. 3(d) and 4 which we interpret to be a strange attractor. There also exists a copy of this object obtained on applying the symmetry operation, $(x,y,z)\rightarrow(-x,-y,-z)$. A Poincaré section taken at the maximal values of x [Fig. 5(a)] yields the return ''map,'' $x_{n+1}=f(x_n)$, shown in Fig. 5(b) (though the plot of x_n against x_{n+1} is evidently not one dimensional, we informally refer to it as a map).

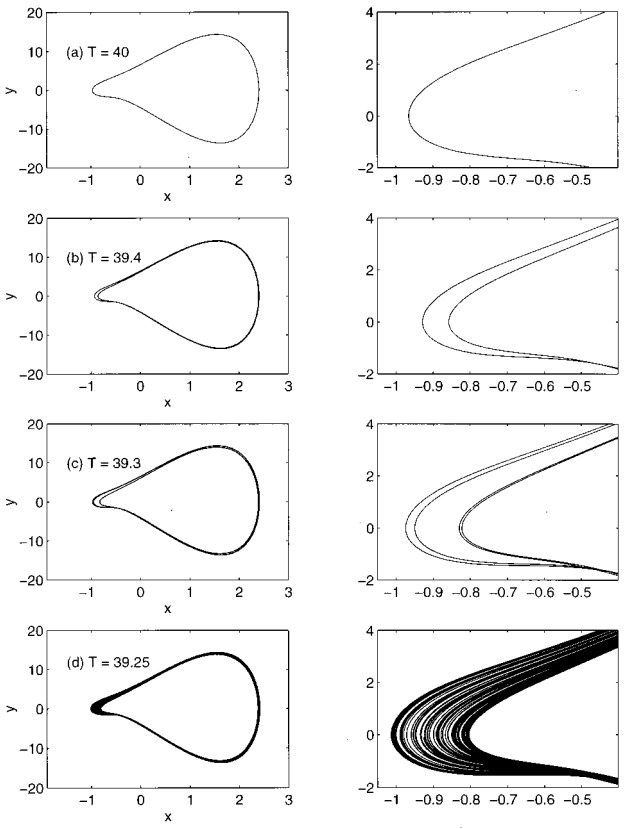

FIG. 3. Period doubling cascade. Shown are orbits projected onto the (x,y) plane for (a) $T=40$, (b) $T=39.4$, (c) $T=39.3$, and (d) $T=39.25$, together with magnifications near the left-hand tip of the attractors.

The run of solutions with the parameter T is shown more fully in the bifurcation diagram of Fig. 6. This shows the

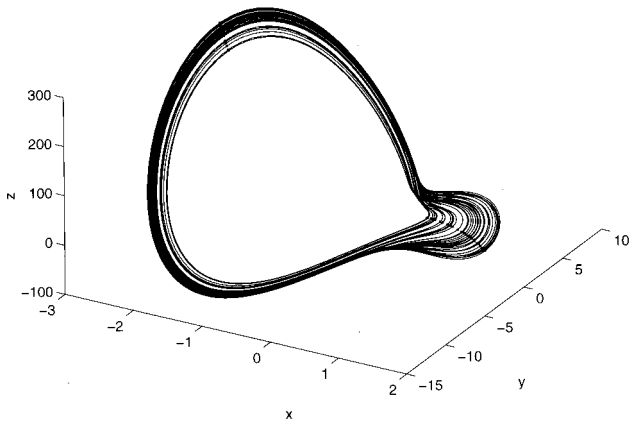

FIG. 4. Attractor at $T=39$ in the phase space (x,y,z). The dots indicate the Poincaré section $y=0$; those with $x>0$ are shown in Fig. 5.

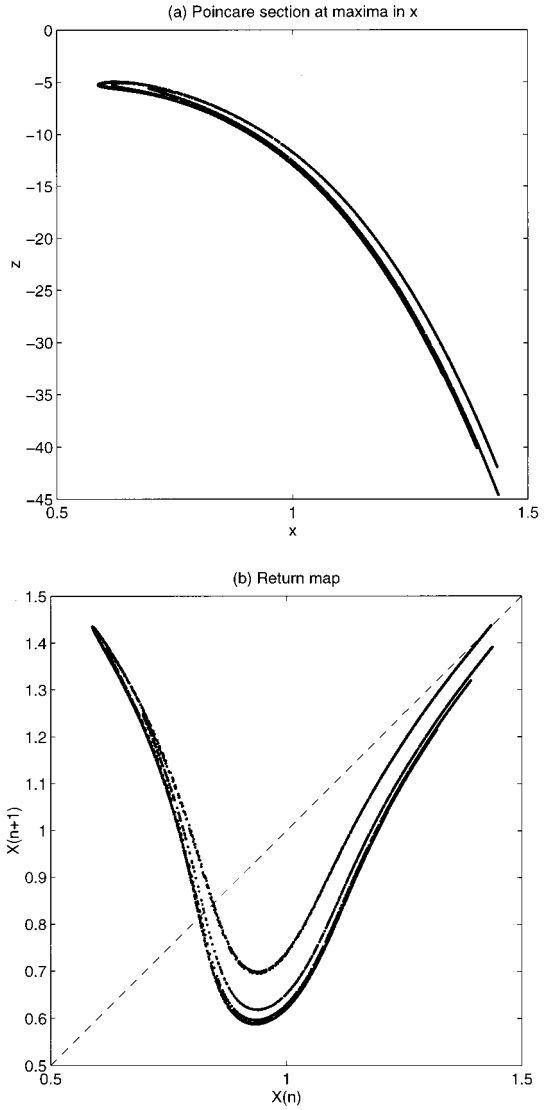

FIG. 5. (a) Poincaré section at the maxima in x of the object shown in Fig. 4 ($T=39$). This gives the maximal values, X_n, which are used to construct the return ''map'' in panel (b).

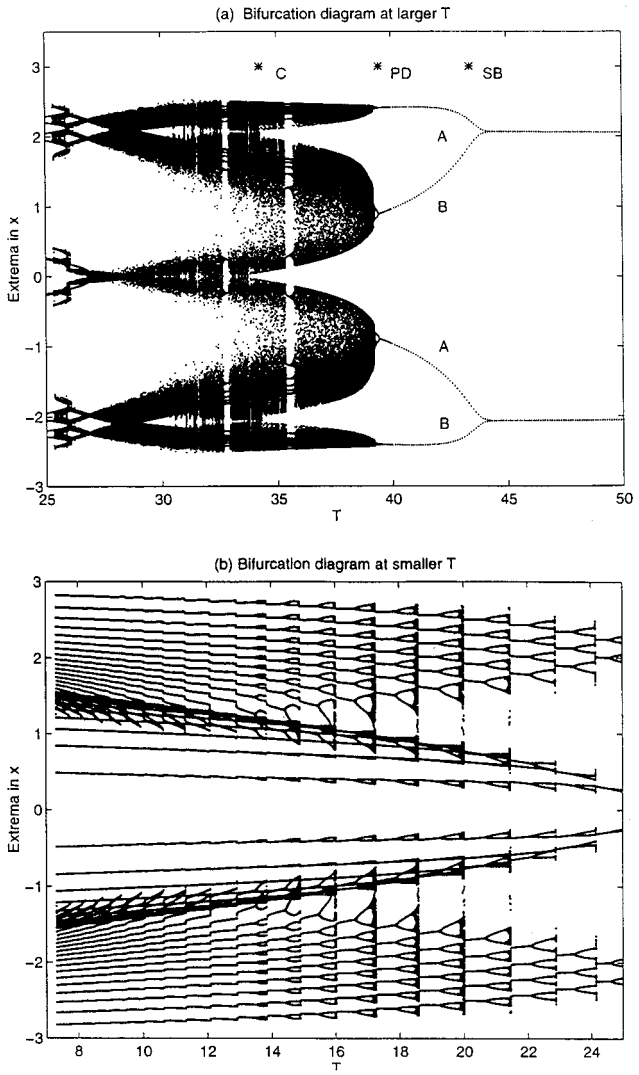

FIG. 6. Bifurcation diagram obtained by recording the extremal points in x ($y=0$) over intervals 200 time units long after transients have largely subsided, for various values of T. Panels (a) and (b) divide the range in T into two. In the first panel, there are two attractors that are mirror images of each other, labeled A and B. The symmetry breaking bifurcation (SB), first period doubling (PD) and merging of the two attractors (C) are also indicated.

extremal values of x explored over a certain time interval (200 units), after transients have subsided, as a function of T.

Beyond the cascade to chaos, the attractor develops as we lower T; in the familiar fashion, windows of stable periodic orbits appear. The most prominent in Fig. 6 is a period-7 window near $T=35.5$. (Note that this does not mean that period-3 never appears; the usual period-3 window is too narrow to pick out in Fig. 6 and the return map of 5 contains period-3 points - see Table II.) At $T\approx 34.25$, the two asymmetrical attractors collide and merge; for smaller T there is a single attractor with symmetrical structure (see Fig. 8).

Eventually, for $T=28$, the region occupied by the attractor again becomes narrow, and the object once more has a ribbonlike structure. More phase portraits are shown in Fig. 8. At smaller T still, a striking pattern appears in the bifurcation diagram consisting of stable limit cycles, period-doubling cascades and small windows of chaos (see Fig. 6). The attractors are rather complicated orbits [see Fig. 1(e) and 1(f)] that wind repeatedly around foci straddling the origin on the x axis [Figs. 1(f) and 8(d)]. But these foci cannot be fixed points.

Note that there are multiple attractors that are not revealed by the bifurcation diagrams in Figs. 6(a) and 6(b). For example, in the detail of Fig. 7, the thicker dots show the location of a stable periodic orbit that coexists with the (presumably) chaotic attractor near $T=20$.

To interpret some of the structure of the bifurcation diagram we now isolate two particular bifurcations of the plethora of Fig. 6.

C. Homoclinic behavior near $T=27$

In Fig. 6, near $T=27$, the attractor collapses to a relatively compact form. A sample phase portrait is shown in

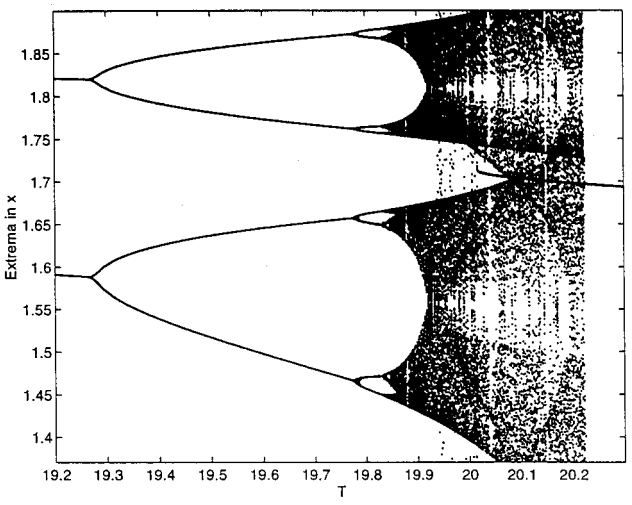

FIG. 7. A detail of the bifurcation diagram. Two separate runs near $T=20$ are shown. In one run, the sequence runs from small T upwards, in the second, from large T downwards. This isolates two coexisting attractors; a strange object signified by the ''cloud'' of dots, and a stable limit cycle portrayed as thicker points near $x=1.7$.

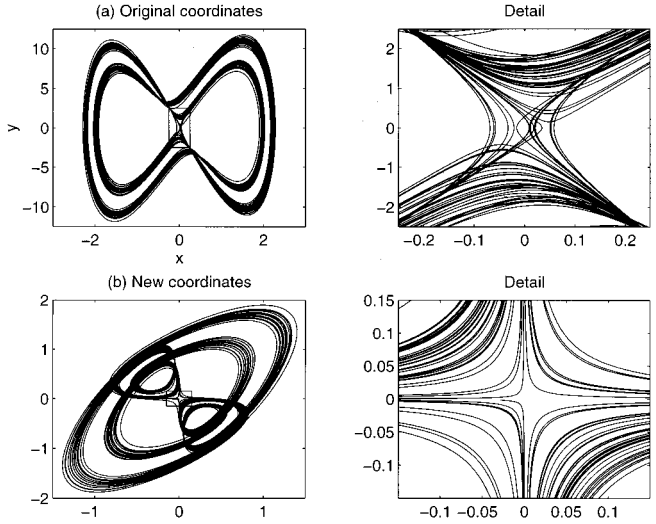

FIG. 9. Numerical evidence for a Lorenz-like flow at $T=27.4$. In panel (a), the phase portrait is shown projected onto the (x,y) plane. In (b), the orbit is drawn projected onto the (e_1,e_2) plane, where e_1 and e_2 are defined by the linearization around the origin. Magnifications of the neighborhood of $x=y=z=0$ are also shown in both cases.

Fig. 8(c). This ribbonlike attractor is composed of two distinct strips or bows stemming from the neighborhood of the origin. Within each strip the orbit circulates comparatively uniformly. However, in the vicinity of the origin, there is a relatively rapid divergence of neighboring trajectories, much as a straining flow in a fluid [see Fig. 9(a); projection on the (x,y) plane obscures this feature somewhat]. This region is of prime importance in controlling the dynamics of the flow.

The form of the attractor also suggests that there is an orbit nearby in parameter space that leaves the origin, winds around one of the bows of the ribbon, then ultimately returns to $x=y=z=0$ (these orbits can be constructed numerically). That is, a nearby homoclinic orbit. In fact, as the following arguments suggest, the dynamics of the system near $T=27$ is much like a ''Lorenz flow'' (e.g., Ref. 7).

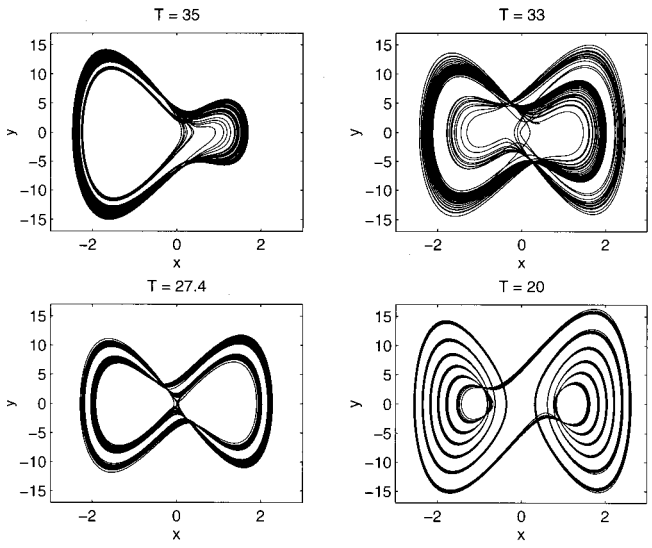

FIG. 8. More chaotic attractors projected onto the (x,y) plane for $T=35$, 33, 27.4, and 20.

Near the origin, we may linearize the equations:

$$\dddot{x}+\ddot{x}-(R-T)\dot{x}+Tx=0. \tag{14}$$

The solutions are $\exp \nu_j t$, for $j=1,2,3$. If $R \gg T$, then

$$\nu_1 \approx -\sqrt{R-T}, \quad \nu_2 \approx \sqrt{R-T}, \quad \text{and} \quad \nu_3 \approx T/(R-T). \tag{15}$$

The ν_j's are the eigenvalues of the flow near the origin. Evidently, $\nu_1<0$, but ν_2 and ν_3 are both negative, although in this limit, $\nu_3 \approx 0$. Associated with the eigenvalues are the vectors, $\mathbf{e}_j$. These eigenvectors locally define the stable and unstable manifolds of the origin.

Provided $R \gg T$, then, we anticipate that the dynamics near $x=y=z=0$ is one composed largely of contraction along the stable direction, $\mathbf{e}_1$, and expansion along the strongly unstable vector, $\mathbf{e}_2$. Numerical confirmation of this view is provided in Fig. 9(b), where we use the vectors $\mathbf{e}_j$ as a coordinate transformation, $(x,y,z) \rightarrow (e_1,e_2,e_3)$, and plot the phase portrait on the (e_1,e_2) plane. The magnification near the origin displays the ''unraveled'' characteristics of the dynamics, and closely resembles the usual structure of a Lorenz flow.

A more quantitative description of the dynamics can be gleaned using standard dynamical systems techniques (e.g., Ref. 7). We consider a local neighborhood of the origin such as the detail of Fig. 9(b); $-c<e_1<c$ and $-c<e_2<c$ for some constant c [equal 0.15 in Fig. 9(b)]. The orbits enter this region from the left or right, then leave through the top

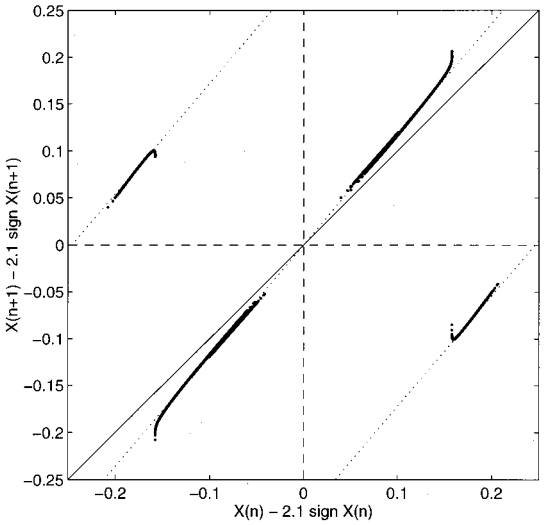

FIG. 10. Return map taken from the Poincaré section, $y=0$, $|x|>2.1$, which corresponds to the two largest of the four extrema of the ''bows'' of the attractor in Fig. 9(a). $T=27.4$. The constants, ± 2.1 have been subtracted from the x values, X_n, to reveal more of the structure of the map. The dotted lines have slope $-\nu_1/\nu_2 \approx 1.175$.

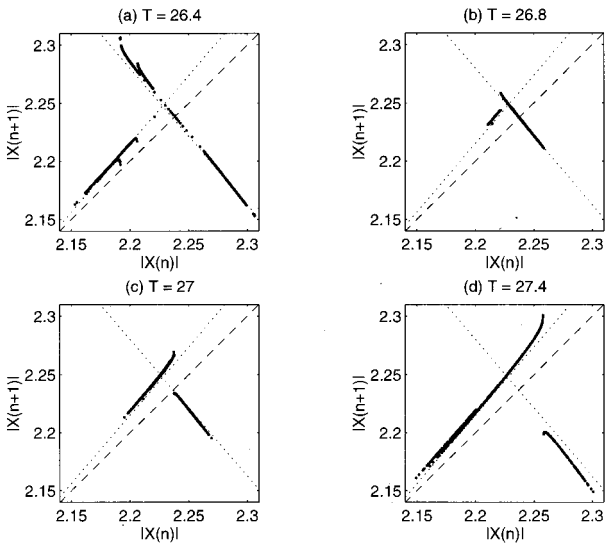

FIG. 11. Various return maps of $|X_n|$, where X_n is taken from Poincaré sections at the primary extrema of the outer arms of the attractors for (a) $T=26.4$, (b) $T=26.8$, (c) $T=27$, and (d) $T=27.4$. In each case we have also included dotted lines with slope, $\pm\nu_1/\nu_2 \approx \pm 1.175$. Note that the map in panel (a) is double-valued; this arises because for T less than the homoclinic value (about 26.9), the attractor is no longer symmetrical, and so taking the absolute value introduces an unnecessary ambiguity.

or bottom of the ''box.'' In line with the observation, $\nu_3 \approx 0$, we ignore the evolution of the coordinate e_3 within the box.

For the nth traversal of the region, we denote the coordinate on the right or left hand edges of the box by $(\pm c, \xi_n)$. Then, the orbit leaves the box at the point $(\xi_*, \pm c)$, where

$$\xi_* = \pm c\,|\xi_n/c|^{-\nu_2/\nu_1} =: \pm c\,|\xi_n/c|^{\sigma}, \tag{16}$$

and we take $-$ or $+$ depending on whether the orbit entered with $\xi_n<0$ or $\xi_n>0$.

The orbit subsequently follows an excursion dictated by the outer arms of the flow. However, the flow here is uncomplicated, and the trajectory becomes reinjected into the box through one of the sides. We assume that the location on the side is simply a function of the previous point of exit; that is, ξ_*. The simplest possible functional form is a linear one, which is approximately valid if the attractor forms a narrow ribbon. Moreover, the attractor we are attempting to represent is symmetrical. Hence we take

$$\xi_{n+1} = \begin{cases} A + B\xi_* & \text{if } \xi_n > 0 \\ -A - B\xi_* & \text{if } \xi_n < 0, \end{cases} \tag{17}$$

where A and B are constants. Whence,

$$\xi_{n+1} = \pm A + c^{1-\sigma} B\,|\xi_n|^{\sigma}. \tag{18}$$

This is a return map on the Poincaré section, $e_2 = \pm c$.

For the case at hand, the ratio, $-\nu_2/\nu_1 = \sigma \approx 1$. Hence the map (18) is approximately composed of a discontinuous linear function with slope near ± 1. In Fig. 10 we show a return map that takes such a form. The section used for this map is $y=0$ and $|x|>2.1$, which corresponds to the largest extrema in x of the outer ribbons of the flow; suitable constants have been subtracted from the resulting x values to reveal the structure. The slopes of the map in Fig. 10 are close to $-\nu_1/\nu_2$, which [though different from what one expects from (18)] reflects the controlling influence of the dynamics near $x=y=z=0$.

We may use the symmetry of the attractor to simplify the return map further; we simply take the absolute value of the coordinates of the section. This leads to a compact map that concisely represents the dynamics [see Fig. 11(d)]. In fact, the bifurcation pathway takes the form of a simple sequence of return maps (Fig. 11). Thus in principle, the dynamics of the system for T near 27 can be predicted by a discontinuous linear map.

D. Solutions at small T

To understand the complicated pattern of bifurcations for $T<25$ [Fig. 6(b)], we focus on a range centered at $T=20$. For this value of T we have the attractor displayed in Figs. 1(e) and 8(d). We cut this attractor with a Poincaré section at $x=0$, and use symmetry to record only $|y|$ and $|z|$ at each intersection. The associated return maps at four values of T are shown in Fig. 12.

Four stages in the bifurcation sequence are illustrated by the maps shown in Fig. 12. For smaller T there is a period doubling cascade centered on a fixed point that corresponds to a symmetrical periodic orbit with six turns about each ''focus.'' This leads to the object represented in Fig. 12(a). This object develops as T increases and the map acquires more structure [see Fig. 12(b)]. Next, in Fig. 12(c), there is a saddle node bifurcation where a new pair of fixed points appear at lower $|z|$; these correspond to periodic orbits with seven turns about each focus. At this stage, there are two

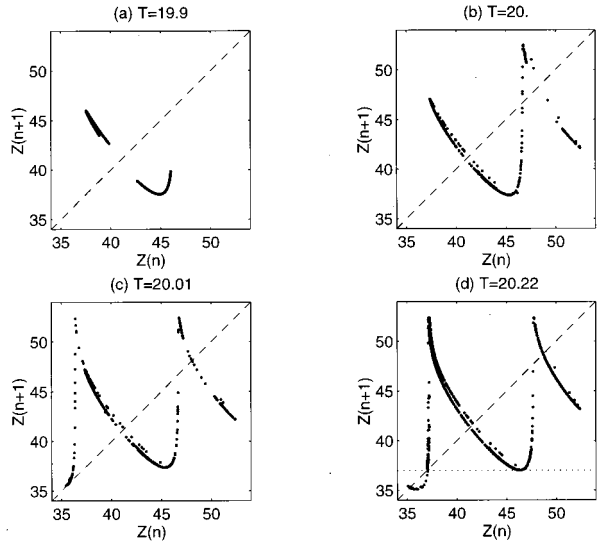

FIG. 12. Return maps on the section $x=0$ for (a) $T=19.9$, (b) $T=20$, (c) $T=20.02$, and (d) $T=20.22$. The maps show $|z_n|$ against $|z_{n+1}|$.

attractors; the new stable fixed point and the original strange attractor. Finally, the chaotic object loses asymptotic stability as its invariant set collides with the newly created unstable fixed point [Fig. 12(d)].

A remarkable feature of the maps shown in Fig. 12 is that the ''curve'' $z_{n+1}=g(z_n)$ is approximately the same in each case up to a T-dependent offset in largely the horizontal. This is shown further in Fig. 13 where we collapse the curves to a common ''function,'' $z'=G(z)$, by including suitable offsets. Moreover, the function is also nearly periodic and can be extended to the right and left. This function can be thought of as an ''empirical return map'' that we may shift horizontally to simulate the bifurcation path. This shift reproduces the repeated appearance of stable orbits, period doubling cascades and chaotic windows of Fig. 6(b). Moreover, it suggests a sequence like that shown in Fig. 14 which plots the fixed points as a function of the horizontal shift.

An important feature of this bifurcation picture is that there is a single periodic orbit that winds through a large number of saddle-node bifurcations as T is decreased. At

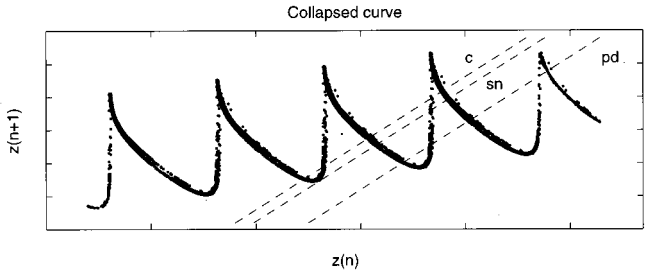

FIG. 13. Composite function, $G(z)$. The action of decreasing T is equivalent to shifting the graph of $G(z)$ to the right; equivalently, this can be viewed as dragging the diagonal line, $z'=z$ to the left, as shown. A period doubling, saddle node, and destruction of the chaotic attractor are indicated.

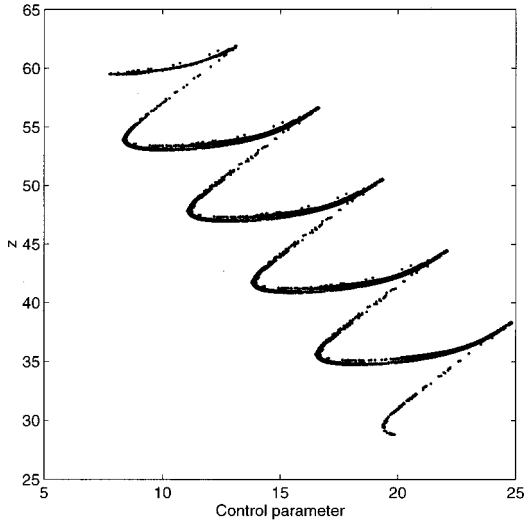

FIG. 14. Bifurcation diagram suggested by the ''empirical map'' of Fig. 13.

each turnaround, the orbit acquires an extra half turn about both foci. In addition, there are period doubling cascades along the path (there must also be inverse period doubling cascades on the right-hand portions of the branches, though these occur over parameter ranges that are too small to observe). This image is reminiscent of Shilnikov theory,[8] although the underlying periodic orbit is not tending to a homoclinic connection. There are also similarities between the bifurcation diagram and map shown above with some of the results portrayed in Ref. 6; these may aid in the interpretation of the ''pre-turbulence'' that occurs in the chaotic regime before the period doubling cascade.

Numerical evidence in support of the scenario of Fig. 14 is shown in Fig. 15. This plots the loci of the lowest-order periodic orbits crossing the Poincaré section $x=0$. Also indicated are points from solving a succession of initial-value

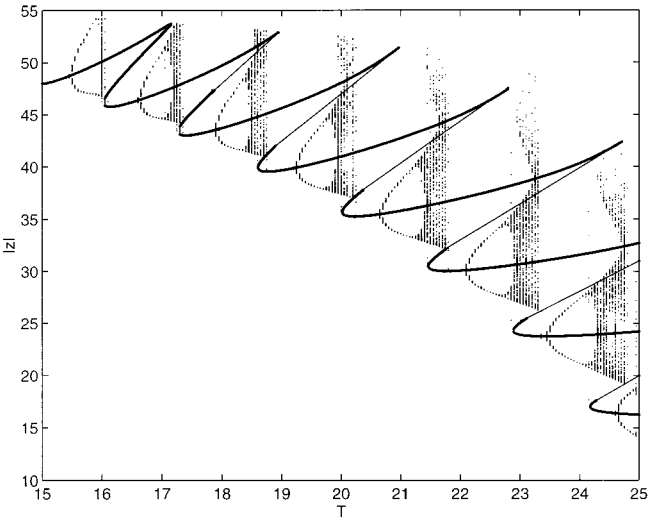

FIG. 15. Actual bifurcation diagram taken from the section $x=0$.

problems. This picture shows the winding of the principal periodic orbit, together with the period doubling cascades (we have not followed the orbits completely around the bifurcation path; near the maxima of the map, the orbits become very unstable and difficult to find).

The geometry of the orbit can be interpreted in terms of Duffing's equation. When $R \gg 1$, we may neglect the term $-Tx$ in the Moore–Spiegel equations, then integrate:

$$\ddot{x}+\dot{x}+Rx\left(\frac{1}{3}x^2-1\right)\approx C, \tag{19}$$

where C is a constant determined from the initial conditions. If $C=0$, solutions of Eq. (19) spiral into the points, $(\pm\sqrt{3},0,0)$. The assumption that the $-Tx$ term is negligible requires $|R(1-x^2)y|<|Tx|$ and for spiraling orbits this is true, on average, until we enter an $O(T/R)$ neighborhood of $(\pm\sqrt{3},0,0)$. The neglected $-Tx$ term then reasserts its influence; the full system in this region is approximated by

$$\dddot{x}+\ddot{x}\approx\pm\sqrt{3}T. \tag{20}$$

Solutions to this equation travel outwards from $(\pm\sqrt{3},0,0)$ roughly along the x axis until $|R(1-x^2)y|>|Tx|$ and we then revert to (19). The solution to (20) drives the orbit away from one of $(\pm\sqrt{3},0,0)$ and into the domain of attraction of the other. Thus the cycle repeats indefinitely.

In principle, we could use matched asymptotic methods to piece together the solutions to (19) and (20), in order to construct a uniformly valid approximation (cf. Ref. 9). This might enable us to fashion an asymptotic return map to parallel the empirical one portrayed in Fig. 13.

III. THE SLAVE SYSTEM

We now consider synchronization of the Moore–Spiegel system. For some dynamical systems, such as the Lorenz equations, one can prove synchronization using a Lyapunov function. For the Moore–Spiegel system in terms of the coordinates (x,y,z), there is no analogous approach and we are unable to demonstrate synchronization rigorously. However, we can show that it is not possible to synchronize using y and z as drive variables. We study the third possibility (x driving) from a numerical perspective.

A. Driving with *z*

We proceed in reverse order and consider driving with the coordinate z first, since this proves to be the simplest case. The slave system takes the form

$$\dot{X}=Y \quad \text{and} \quad \dot{Y}=z. \tag{21}$$

It is apparent that the important dynamical equation has been completely lost in this substitution. Moreover, the solution can be written as

$$\begin{aligned} &X=X(0)+[Y(0)-y(0)]t+x(t)-x(0) \quad \text{and} \\ &Y=Y(0)+y(t)-y(0), \end{aligned} \tag{22}$$

which indicates that Y never synchronizes if there is an initial separation, and X diverges.

B. Driving with *y*

Next, consider driving with y. Then the slave system takes the form

$$\dot{X}=y \quad \text{and} \quad \dot{Z}=-Z-(T-R+RX^2)y-TX. \tag{23}$$

If we define the differences,

$$\Delta_x=X-x \quad \text{and} \quad \Delta_z=Z-z \tag{24}$$

(we will use this notation henceforth, including also $\Delta_y=Y-y$ and so forth), then the equations reduce to

$$\dot{\Delta}_x=0 \quad \text{and} \quad \dot{\Delta}_z=-\Delta_z-R\Delta_x(2x+\Delta_x)y-T\Delta_x. \tag{25}$$

Hence $\Delta_x=\Delta_x(0)$ and

$$\begin{aligned} \Delta_z=&[\Delta_z(0)-T\Delta_x]e^{-t}+T\Delta_x-R\Delta_x \\ &\times\int_0^t[2x(t')+\Delta_x]y(t')e^{t'-t}dt'. \end{aligned} \tag{26}$$

Thus the system cannot synchronize unless $\Delta_x(0)=0$. Then, in fact, the system synchronizes whatever the initial separation, $\Delta_z(0)$.

An important feature of the slave system with y driving is that the difference in x does not evolve. This suggests a remarkable coordinate change: let $x'=x$, $y'=y+\varpi x$ and $z'=z$. In terms of the new variables, the system is written,

$$\dot{x}=y'-\varpi x, \quad \dot{y}'=z+\varpi y'-\varpi^2 x \tag{27}$$

and

$$\dot{z}=-z-(T-R+Rx^2)(y'-\varpi x)-Tx. \tag{28}$$

If we now synchronize two of the transformed systems using the variable y', then the differences evolve according to

$$\dot{\Delta}_x=-\varpi\Delta_x \tag{29}$$

and

$$\begin{aligned} \dot{\Delta}_z=&-\Delta_z-R\Delta_x(2x+\Delta_x)y-[T-\varpi(T-R)]\Delta_x \\ &+\varpi R(\Delta_x+x)^2\Delta_x. \end{aligned} \tag{30}$$

Now, $\Delta_x=\Delta_x(0)e^{-\varpi t}$, and so $\Delta_x\to 0$ as $t\to\infty$, provided $\varpi>0$. Moreover, the forcing terms on the right-hand side of Eq. (30) also decay exponentially in this limit. Hence also $\Delta_z\to 0$. Thus the system always synchronizes.

The possibility of using a linear transformation of variables to generate a new, synchronizable system has been explored in Ref. 2 (see also Ref. 10). This thread will recur later, but next we attack the problem of the slave with x driving by brute force.

C. Driving with *x*

Finally, we deal with the case of driving with x. The slave system is

$$\dot{Y}=Z \quad \text{and} \quad \dot{Z}=-Z-(T-R+Rx^2)Y-Tx; \tag{31}$$

equivalently, $\Delta_z=\dot{\Delta}_y$ and

$$\ddot{\Delta}_y+\dot{\Delta}_y+(T-R+Rx^2)\Delta_y=0. \tag{32}$$

That is, the difference Δ_y evolves as the displacement of a damped oscillator with a time-varying spring constant. We cannot, in general, demonstrate synchronization or lack of it in this equation. Hence synchronization is not obvious, and numerical experiments are needed to settle the score. This situation is somewhat similar to that occurring for the Rössler system.[1]

When $x(t)$ converges to a limit cycle, Eq. (32) is like a Mathieu equation; the question of synchronization amounts to the resolution of a Floquet problem. Specifically, (32) has two solutions of the form, $F_j(t)e^{\mu_j t}$, for $j=1,2$, where the functions, $F_j(t)$, are periodic with the same period as the driving limit cycle. The μ_j's are Floquet exponents. If both μ_1 and μ_2 are negative, the system synchronizes.

In addition, the linear operator in (32) can be recast in matrix form, from which the trace condition

$$\mu_1+\mu_2+1=0 \tag{33}$$

follows. Hence at least one of the μ_j's must be negative. Note that these exponents can be defined even if the limit cycle is unstable.

The exponents μ_j are *not* the same as the Floquet exponents that arise from studying the orbital stability of the limit cycles themselves. That Floquet calculation leads to the *orbital stability exponents*, λ_k, $k=1,2,3$. Of these, one must be identically zero as a consequence of the translational invariance of the system. To distinguish the two kinds of exponents, we refer to the μ_j's as the *synchronization stability exponents*.

When $x(t)$ is a chaotic signal, ascertaining synchronization constitutes a generalized kind of Floquet calculation. In this case, there is no separation of the solution into a periodic part and an exponential. However, for large t, $\Delta_y \sim e^{\hat{\mu}_j t}$, $j=1,2$. Now, though, the $\hat{\mu}_j$'s are Lyapunov exponents. Note that the relation (33) will still hold. Once again, these exponents are different from the Lyapunov exponents measuring the exponential rate of divergence of neighboring trajectories on the attractor itself. We denote the latter by $\hat{\lambda}_k$, $k=1,2,3$, and use the terminology, *synchronization Lyapunov exponents* and *orbital Lyapunov exponents*, respectively. The synchronization exponents are also referred to as *conditional Lyapunov exponents* in the literature.[1]

In Fig. 16 we present numerical results for the leading orbital Lyapunov exponents over the familiar range of T. Also shown are the largest orbital stability exponents of the symmetrical and asymmetrical, period-one limit cycles. The pattern of chaotic windows at smaller T are signified by spikes in the exponent.

In Fig. 17 we show the analogous results for the leading synchronization Lyapunov exponents. Once again we include the analogous exponents for the two lowest period orbits; where these orbits are stable, the synchronization Lyapunov and stability exponents are in agreement. The regimes in which we expect synchronization with x driving are clear from this picture: synchronization fails around the period-doubling cascade, then again for smaller T.

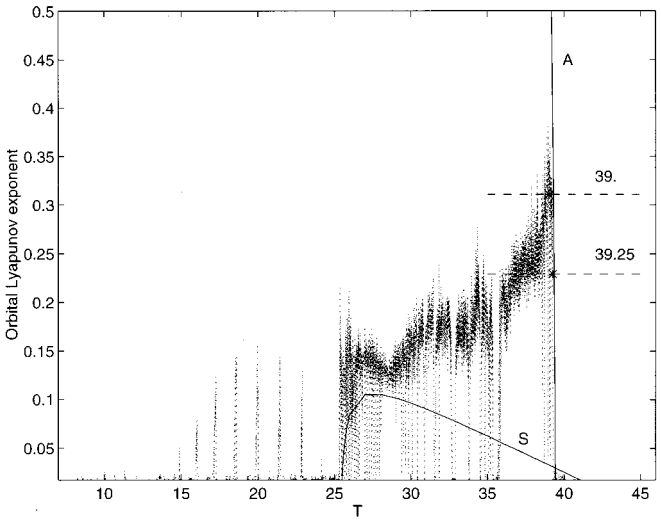

FIG. 16. Leading orbital Lyapunov exponent against T. Dotted lines show numerically determined exponents. The solid lines labeled S and A denote the leading orbital stability exponents of the symmetrical and asymmetrical period-one limit cycles. The points at $T=39.25$ and $T=39$ are derived from the periodic orbit expansion of Sec. IV. Note that where there is a stable periodic orbit, the leading exponent is zero.

Notably, synchronization fails when T drops below about 27.4. This is the parameter range in which the attractor considered in Sec. II C appears. The reason why synchronization fails in this case is related to the fact that the flow in the vicinity of the origin plays a critical role in determining the dynamics of the system for this attractor. Near $x=y=z=0$ we have an unstable manifold of two dimen-

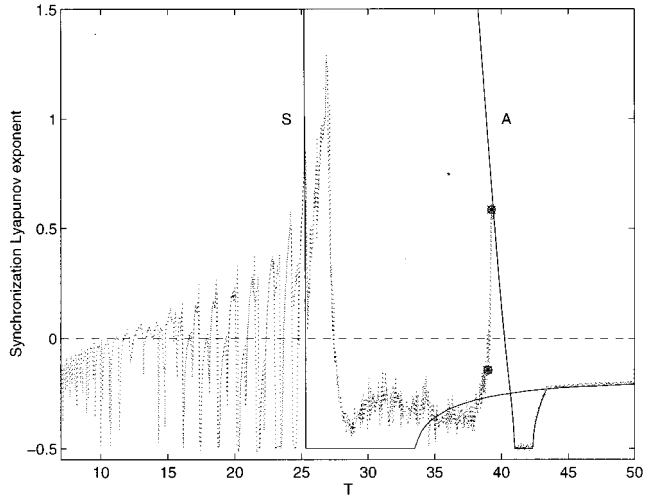

FIG. 17. Leading synchronization Lyapunov exponent against T. The dotted lines show numerical calculations. There are two cases drawn, one derived starting at small T and working up, the other at large T and working down. Their difference signifies the presence of multiple attractors (particularly over the range $20<T<25$). The solid lines labeled S and A denote the leading synchronization stability exponents of the symmetrical and asymmetrical period-one limit cycles. The points at $T=39.25$ and $T=39$ are derived from the periodic orbit expansion of Sec. IV.

sions. Hence the synchronization of an arbitrary coordinate in this case, could in principle prevent the master and slave from diverging from one another along one of the unstable directions, but not the other. Hence synchronization is doomed to fail (though a clever linear transformation should work, see Ref. 2).

For smaller T, there are multiple attractors (the exponent plotted in Fig. 17 is actually taken from two computational runs, one beginning at large T and working down, the other for small T and working up; this goes some way towards capturing the ramifications of multiplicity of the attractors). The synchronization of the systems here depends on whether the attractor is periodic or chaotic; where cycles are stable, they are typically synchronizing. This property is lost in the period doubling cascades and when the orbits disappear in saddle-node bifurcations. The chaotic windows are mostly desynchronizing. We have not explored this in further detail.

IV. PERIODIC ORBIT EXPANSIONS

The calculations of the last section were largely brute force numerics in nature. We were forced into this because it was not possible to rigorously establish whether the slave with x driving was synchronizable. Now we attempt to take a more elegant tack, and use a periodic orbit expansion to derive the synchronization properties from a more natural basis.

A. Cycles

A strange attractor can be viewed as a set of an infinite number of unstable periodic orbits. That is, these orbits are the skeleton of the attractor around which the system is evolving. In fact, an original vision of chaos in the Moore–Spiegel oscillator was that the system wandered incessantly among the neighborhoods of unstable limit cycles.[5] Lately this image has acquired more quantitative meaning in terms of a periodic orbit expansion.[11,12]

The expansion represents the attributes of the attractor in terms of the properties of the periodic orbits. The aim is to derive statistical chaotic averages by suitably summing over the cycles. This kind of technique is a natural way to compute quantities such as Lyapunov exponents, one simply formulates an appropriate average over the Floquet exponents of the cycles. For this particular measure of chaos, the calculation amounts to the following construction.

The initial step is an organization of the periodic orbits. First, we discard periodic orbits that are simply multiples of smaller period orbits (that is, multiple encirclings of the same orbits). This leaves us with a set of distinct ''prime'' orbits. For simple attractors, the prime orbits can often be conveniently labeled according to their ''order''; that is, the approximate integral number of periods of the simplest limit cycle, or the number of distinct maxima in x (thus the periodic orbits in Fig. 3 are order 1, 2, and 4). Moreover, one can usually attach symbolic labels to the orbits and use symbol dynamics to find and concisely classify them. In fact, the ''map'' shown in Fig. 5 indicates that the orbits can be organized according to a relatively simple binary alphabet. The letters of the alphabet, 0 and 1, follow from whether the value of x on the section (the ''bounce'' of the orbit) lies to the right or left of the minima of the ''curves'' of the ''map'' (this is not quite the case, but for the lowest period orbits, this categorization suffices).

TABLE I. Periodic orbit information for $T=39.25$. Accuracy check: $\zeta=-0.0197$.

Order	Symbolic coding	Λ	M	Period
1	1	1.8088	2.9147	1.5221
2	01	1.9073	4.8763	3.0001
4	0111	3.5245	29.224	6.0166
6	001011	8.4948	217.84	9.0499
6	001111	8.1771	172.81	9.0320
8	01111111	18.234	1747.0	12.089
8	00010101	17.795	1508.7	12.078
8	00000101	12.574	762.21	12.025

For $T=39.25$ and $T=39$, we then obtain the lowest-order, prime periodic orbits that are listed in Tables I and II. Also listed are the symbol codings, the period, τ, and the leading orbital and synchronization stability eigenvalues, Λ and M. These latter quantities are related to the Floquet exponents:

$$\Lambda=\exp\,\lambda_1\tau \quad \text{and} \quad M=\exp\,\mu_1\tau, \tag{34}$$

TABLE II. Periodic orbit information for $T=39$. Accuracy check: $\zeta=0.0032$.

Order	Symbolic coding	Λ	M	Period
1	1	3.144	4.0950	1.5574
2	01	5.717	4.3394	3.0115
3	001	8.552	1.2111	4.3311
3	011	21.79	14.011	4.5459
4	0001	9.749	0.2627	5.5935
4	0011	30.01	3.2028	5.8302
4	0111	57.40	58.94	6.1074
5	00001	9.756	0.0757	6.8271
5	00011	29.35	0.6143	7.0483
5	00101	35.98	5.8512	7.3421
5	00111	48.844	12.071	7.3913
5	01011	121.92	64.624	7.5629
5	01111	188.20	238.01	7.6630
6	000001	8.631	0.0680	8.0453
6	000011	22.70	0.2401	8.2257
6	001101	127.88	22.132	8.8840
6	001111	172.07	49.053	8.9446
7	0000001	5.335	0.0859	9.2637
7	0000011	11.09	0.1674	9.3645
7	0001001	79.158	0.3370	9.9229
7	0001011	165.56	2.1810	10.0740
7	0010111	323.66	52.832	10.4090
7	0011101	364.58	89.296	10.4433
8	00001001	66.365	0.1458	11.1539
8	00001011	111.06	0.5854	11.2564
8	00100101	333.15	6.9288	11.6728
8	00100111	495.46	16.056	11.7307
8	00100011	578.20	7.6902	11.5930
8	00101101	829.69	87.118	11.8971

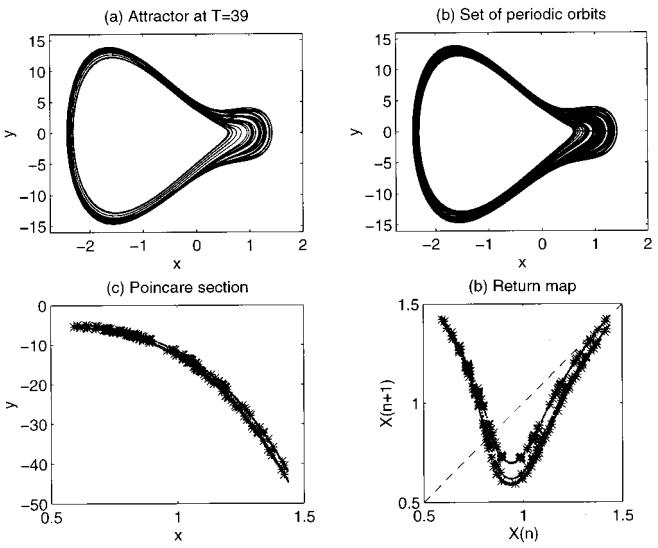

FIG. 18. Representation of the attractor by periodic orbits at $T=39$. Panels (a) and (b) show phase portraits of the attractor and collection of limit cycles used in the expansion. Panels (c) and (d) show the usual section and return map with the periodic points superposed.

where we order the exponents such that λ_1 and μ_1 are the largest. Shortly we will also add the subscript p to distinguish the orbits.

It turns out that for $T=39$, there are period-6 and period-7 orbits with anomalously small stability eigenvalues. That is, there are high-order orbits that are unusually stable. The expansion should in principle be carried out to include all orbits up to and including at least these orders. We include those listed in Table II, though we have made no attempt to ensure that we have not missed some of the strongly unstable, higher-order orbits; there is an accuracy check that gives us confidence that any error is small (and permits us to proceed without undue sophistication in finding the orbits). We have also omitted the symmetrical period-1 orbit since it lies outside the attractor, and ignored the coexisting mirror image. We could use symbol dynamics and ''pruning'' in tandem with explicit symmetry considerations to put this on a more rigorous basis.[13]

For $T=39$, we show the attractor and its representation in terms of the limit cycles in Fig. 18. Note that were we not able to include the anomalously stable pairs of period-6 and period-7 orbits, then there would be a noticeable lack of coverage of the attractor, section and map, particularly in the region corresponding to the right-hand edge and maximum of the map.

B. Expansion

Back to the expansion. A key feature of the cycle expansion is to organize and truncate the sum based upon the order of the orbits. Given orbits of order p and q, we assign order $p+q$ to their ''product,'' and organize that product in the same basket as the order $p+q$ order orbits. Then we assume a certain truncation in order, N, and deal only with orbits and their products up to and less than N.

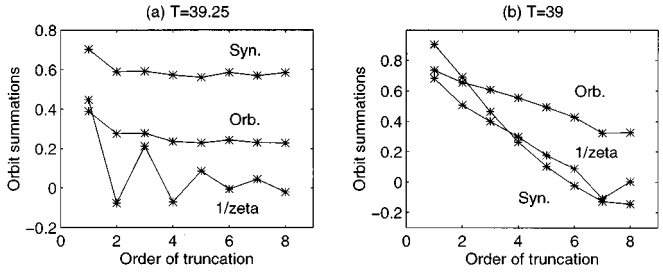

FIG. 19. Periodic orbit sums showing the convergence of ζ^{-1} to zero and the other sums to the orbital and synchronization Lyapunov exponents for (a) $T=39.25$ and (b) $T=39$.

The averaging formulas take the form of sums, denoted Σ', over all, nonrepeating combinations of prime orbits:

$$\frac{1}{\zeta}=1+\sum_{p_1+\cdots+p_k}{}' \frac{(-1)^k}{|\Lambda_{p_1}\cdots\Lambda_{p_k}|}=0 \tag{35}$$

and

$$\hat{\lambda}=\frac{1}{\langle\tau\rangle}\sum_{p_1+\cdots+p_k}{}' (-1)^k\frac{\ln|\Lambda_{p_1}|+\cdots+\ln|\Lambda_{p_k}|}{|\Lambda_{p_1}\cdots\Lambda_{p_k}|}, \tag{36}$$

where

$$\langle\tau\rangle=\sum_{p_1+\cdots+p_k}{}' (-1)^k\frac{\tau_{p_1}+\cdots+\tau_{p_k}}{|\Lambda_{p_1}\cdots\Lambda_{p_k}|}, \tag{37}$$

and for the k^{th} orbit of order p, denoted p_k, the largest stability eigenvalue is Λ_{p_k} and τ_{p_k} is its period.

For example, for the orbits listed in Table (I) at $T=39.25$:

$$\frac{1}{\zeta}\approx 1-\frac{1}{|\Lambda_1|}-\frac{1}{|\Lambda_{01}|}+\frac{1}{|\Lambda_1\Lambda_{01}|}-\frac{1}{|\Lambda_{0011}|} \tag{38}$$

and

$$\hat{\lambda}\approx\frac{1}{\langle\tau\rangle}\left[\frac{\ln|\Lambda_1|}{|\Lambda_1|}+\frac{\ln|\Lambda_{10}|}{|\Lambda_{01}|}-\frac{(\ln|\Lambda_1|+\ln|\Lambda_{10}|)}{|\Lambda_1\Lambda_{01}|}+\frac{\ln|\Lambda_{0011}|}{|\Lambda_{0011}|}\right], \tag{39}$$

where

$$\langle\tau\rangle\approx\frac{\tau_1}{|\Lambda_1|}+\frac{\tau_{10}}{|\Lambda_{01}|}-\frac{(\tau_1+\tau_{10})}{|\Lambda_1\Lambda_{01}|}+\frac{\tau_{0011}}{|\Lambda_{0011}|}, \tag{40}$$

up to fourth order.

The first of the sums corresponds to probability conservation. It may be used as a check on the convergence of the expansion (see for example, Fig. 19). For $T=39.25$, convergence is adequate, less so at $T=39$. The reason is simply the influence of the relatively stable, high-order orbits.

In a similar vein, we can define an orbit expansion for the synchronization Lyapunov exponent:

$$\hat{\mu}=\frac{1}{\langle\tau\rangle_{p_1+\cdots+p_k}}{\sum_{p_1+\cdots+p_k}}'(-1)^k\frac{\ln|M_{p_1}|+\cdots+\ln|M_{p_k}|}{|\Lambda_{p_1}\cdots\Lambda_{p_k}|}. \qquad (41)$$

The orbit sums for both orbital and synchronization Lyapunov exponents are shown in Fig. 19. These sums suggest that $\hat{\lambda}\approx 0.229$ and $\hat{\mu}\approx 0.585$ at $T=39.25$, and $\hat{\lambda}\approx 0.327$ and $\hat{\mu}\approx -0.144$ at $T=39$. These points are plotted in Figs. 16 and 17, where they show agreement with direct numerical evaluations.

In practical terms, it is computationally easier to evaluate exponents numerically rather than via periodic orbit expansion. This becomes especially so for smaller T, when the attractor develops, and the structure of the set of periodic orbits becomes more convoluted. One might then ask the question of how useful the exercise has been.

However, the point of the expansion is that it can provide additional insight. The orbits are tools that we may use to pick apart the attractor. Somewhat surprisingly, one's first guess based on the orbital expansion for synchronization turns out to be wrong. That is, the lowest-order periodic orbits that typically dominate the statistical averages all have synchronization stability eigenvalues greater than one. Thus one can never synchronize to the simplest bones of the attractor's skeleton. In fact, the orbits that contribute most to the synchronization exponent are those with many bounces on the right-hand side of the map in Fig. 18. (equivalently, orbits with symbolic designations containing many 0's in Table II). These orbits are the relatively stable ones at $T=39$, which is why they have such a dominant effect. But it is surprising that the system still synchronizes as we lower T and the structure of the periodic orbits changes.

Note that the synchronization Lyapunov exponent does not reverse sign in an erratic fashion (except for values of T in the range 15–25). Overall, the synchronization exponent is a somewhat less complicated function of T than the orbital exponent $\hat{\lambda}$. Hence we have some grounds for believing that synchronization occurs over entire ranges of T and does not suddenly disappear for isolated, narrow windows in T.

The main lesson of the periodic orbit expansion is that the features of the attractor that determine the synchronization properties are certainly not transparent; chaotic averages can have a convoluted origin. For synchronization exponents, the average is over competing periodic orbits. Hence it would be exceedingly difficult to predict synchronization from any simple criterion. However, this is practically all that the expansion tells us overall, other than the explicit evaluation of the exponents.

V. COORDINATE TRANSFORMATIONS

In the considerations of Sec. III, we pointed out that one could not generally synchronize the Moore–Spiegel system with certain coordinates. Indeed synchronization for x driving depended upon the parameters within the model; this is a relatively common phenomenon found in several other nonlinear systems. Yet with a suitable coordinate transformation in Sec. III B, we could generate a system that always synchronized. We now consider this further.

In Sec. I C we introduced the alternative coordinate system (x,y,λ), where λ and z are related via the *nonlinear* coordinate transformation (7). In the alternative coordinates, the two systems take the form of (8) and (9). Though the master system that we may construct from these new equations is identical with the original oscillator, when we take the new coordinates as drive variables, the slave systems are rather different from those considered in Sec. III. We consider these slave systems in more detail, but it is convenient, and more insightful, to do this from the viewpoint of the generalized potential systems of which the transformed Moore–Spiegel system is a special case.

For the generalized potential systems, the uncoupled equations take the form,

$$\dot{x}=y, \quad \dot{X}=Y, \qquad (42)$$

$$\dot{y}=-V_x(x,\lambda)-\nu y, \quad \dot{Y}=-V_X(X,\Lambda)-\nu Y, \qquad (43)$$

and

$$\dot{\lambda}=-\epsilon[\lambda+g(x)], \quad \dot{\Lambda}=-\epsilon[\Lambda+g(X)], \qquad (44)$$

where ν and ϵ are positive constants, $g(x)$ is a polynomial, and the potential $V(x,\lambda)$ is

$$V(x,\lambda)=\frac{x^m}{m}-\sum_{k=1}^{m-1}\alpha_k(\lambda)\frac{x^k}{k}, \qquad (45)$$

with m an integer.

If we synchronize master and slave in x, then

$$\dot{Y}=-\frac{\partial V(x,\Lambda)}{\partial x}-\nu Y, \quad \dot{\Lambda}=-\epsilon[\Lambda+g(x)]; \qquad (46)$$

the differences evolve according to

$$\begin{aligned}\dot{\Delta}_\lambda&=-\epsilon\Delta_\lambda,\\ \dot{\Delta}_y&=\sum_{k=1}^{m-1}[\alpha_k(\Delta_\lambda+\lambda)-\alpha_k(\lambda)]x^{k-1}-\nu\Delta_y.\end{aligned} \qquad (47)$$

Thus $\Delta_\lambda\to 0$, and so $\Lambda\to\lambda$, as $t\to\infty$. In addition, provided $\nu\neq 0$, $Y\to y$ and the systems synchronize independently of parameter values and initial conditions (unless the slave diverges in finite time, which seems unlikely).

If $\nu=0$, however, which is the case for the Moore–Spiegel oscillator, we have only that $\dot{\Delta}_y\to 0$ as $t\to 0$. Hence Y synchronizes with y to within a constant offset; that is, $Y\to y+c$ where c is a constant determined by the initial condition. This somewhat restricted form of synchronization may be as good as the real thing in many situations (cf. Ref. 15). In any case, the slave will always reproduce the complicated dynamics of the master; it is simply offset.

If we next drive the slave system with y, then we find

$$\dot{X}=y \quad \text{and} \quad \dot{\Lambda}=-\epsilon[\Lambda+g(X)]. \qquad (48)$$

Equivalently,

$$\dot{\Delta}_x = 0 \quad \text{and} \quad \dot{\Delta}_\lambda = -\epsilon[\Delta_\lambda + g(x+\Delta_x) - g(x)]. \tag{49}$$

The situation is now very similar to Sec. III B in that the difference $\dot{\Delta}_x$ does not evolve. So synchronization fails. However, we now adopt the change of variable $y' = y + \varpi x$, where ϖ is real and positive, as in Sec. III B, and drive the system with y'. We are then led to the evolution equations,

$$\dot{\Delta}_x = -\varpi \Delta_x, \quad \dot{\Delta}_\lambda = -\epsilon[\Delta_\lambda + g(\Delta_x + x) - g(x)]. \tag{50}$$

Thus $X \to x$ and $g(\Delta_x + x) \to g(x)$ for $t \to \infty$, and synchronization is ensured.

Finally, driving with λ produces a complicated nonlinear equation for the differences:

$$\dot{\Delta}_x = \Delta_y, \quad \dot{\Delta}_y = -[V_X(X,\lambda) - V_x(x,\lambda)] - \nu \Delta_y. \tag{51}$$

In this case we cannot extract any general results about synchronization. The system may synchronize or not depending upon parameter values, just as for the case we treated in Sec. III C, and possibly even on the initial condition.

To summarize, once one writes the system in a suitable form, there are two synchronizing coordinates (or two up to a constant offset if $\nu = 0$). It is noteworthy that the changes of variable we have used are nonlinear ones, in contrast to the linear transformations considered in Ref. 2. It is also worth emphasizing that this generalized potential viewpoint has identified two synchronizing coordinates for a wide class of nonlinear systems.

VI. FINITE TIME-STEP SYNCHRONIZATION

We have now dealt in some detail with the synchronization properties of the Moore–Spiegel system, based upon the idea of master-slave coupling. However, this is not the only possible way to couple the systems in order to synchronize them. A second possibility, which is similar in flavor but not in mathematical detail, is to solve a succession of initial-value problems in which one evolves the slave for a fixed interval of time, then afterwards resets one of the coordinates (the analogue of the drive variable) and begins anew. This finite-step form of synchronization was introduced in Ref. 16 and appears to work for the Lorenz equations in some parameter regimes. From the mathematical point of view it is difficult to establish any general results about this alternative prescription, and here we settle for a relatively light discussion.

We consider the possibility of synchronizing the Moore–Spiegel system using finite-step resetting of the coordinate x. We select this variable since, without a coordinate transformation, we have seen that it can conceivably act as a successful drive, whereas y and z cannot.

Once again we will use exponents to quantify synchronization. For the finite-step prescription we may define a synchronization exponent according to the following procedure. We take a trajectory of the master system $[x(t), y(t), z(t)]$, and then consider a nearby slave trajectory $[X(t), Y(t), Z(t)]$. Provided the two orbits are close, we may linearize the slave equations about the master orbit; infinitesimal differences evolve according to

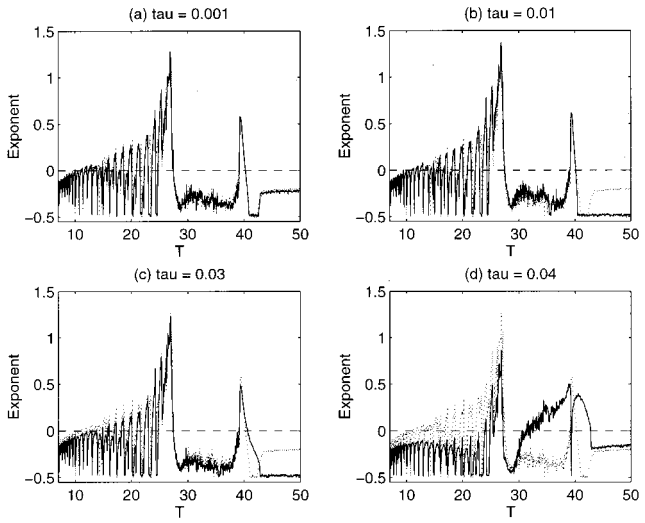

FIG. 20. Finite-step synchronization exponent against T for (a) $\tau = 0.001$, (b) $\tau = 0.01$, (c) $\tau = 0.03$, and (d) $\tau = 0.04$. Also shown by the dotted lines is the leading synchronization exponent for the continuous form of master-slave synchronization. These calculations are conducted beginning at large T and working down, taking the final point from the calculation at the previous value of T as the initial point.

$$\dot{\delta}_x = \delta_y, \quad \dot{\delta}_y = \delta_z,$$

$$\dot{\delta}_z = -\delta_z + (R - T - Rx^2)\delta_y - (2Rxy + T)\delta_x. \tag{52}$$

We evolve this equation between $n\tau$ and $(n+1)\tau$ with $n = 1,2,\ldots$, where τ is the resetting interval, subject to the initial conditions, $\delta_x(n\tau) = 0$ and continuity in δ_y and δ_z. Then, as $t \to \infty$, $(\delta_y, \delta_z) \sim e^{\tilde{\mu} t}$, where $\tilde{\mu}$ represents the leading finite-step synchronization exponent (there are three in total).

One noteworthy point about Eq. (52) is that it is identical to the equations one solves for the orbital Lyapunov exponents of the master system itself (modulo initial values). However, there is no obvious connection between the Lyapunov exponents and $\tilde{\mu}$. When the master system follows a stable periodic orbit, the Lyapunov exponents are negative and one expects perturbations about the orbit to decay. Hence it is not unreasonable to suspect that where there are stable orbits, $\tilde{\mu}$ is negative and the slave synchronizes. This is verified in Fig. 20, which shows calculations of the exponent $\tilde{\mu}$ for four values of τ. The interesting aspect of the calculation is that synchronization occurs even where the orbital Lyapunov exponent is positive (that is, where there is chaos).

On comparing the exponents with the corresponding ones for the continuous version considered in Sec. III, it also appears as though the finite-step prescription can be more effective; by judiciously choosing τ, we may synchronize the systems over almost the whole range in T, and often with faster convergence.

However, there is a serious deficiency in the calculations shown in Fig. 20 and their interpretation. The exponents are

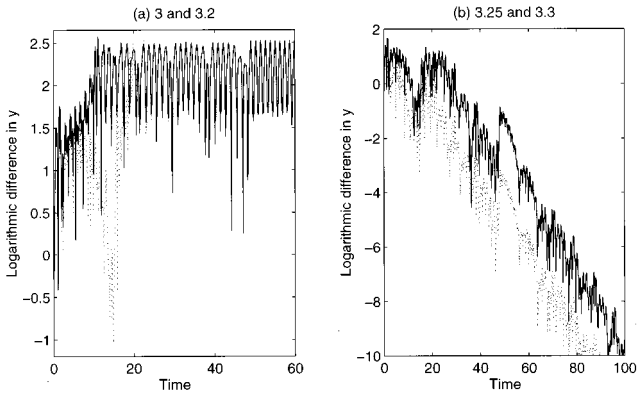

FIG. 21. The logarithm (base 10) of the absolute difference between y and Y for four calculations at $T=35$ with slightly different initial conditions. The initial conditions are $X=x$ and $(Y,Z)=q(1,1)$ for $q=3$, 3.2, 3.25, and 3.3, with (x,y,z) a given point on the master's attractor.

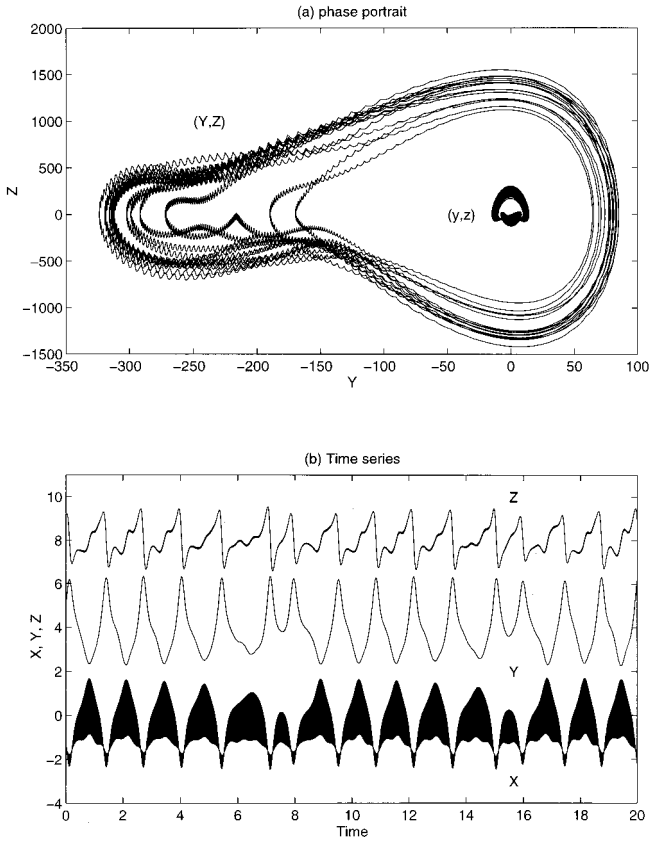

FIG. 22. (a) Phase portrait and (b) time series for the slave system at $T=35$ with initial condition $X(0)=x(0)$ and $Y(0)=Z(0)=3.3$. In (a), the phase portrait of the master system is also shown. In (b), Y and Z are shown scaled and offset.

based on the linear stability of the orbit of the master system. This kind of calculation completely ignores the possibility that this trajectory is unstable to finite amplitude perturbations and that there are other attractors in the slave system. [Such a possibility plagues any synchronization prescription based on linear theory; the continuous case considered in Sec. III fortuitously took a linear form for the differences and so there was no such problem.] In fact, in the current problem, synchronization shows a pronounced dependence on the initial condition. This is brought out in Fig. 21 which shows the (nonlinear) evolution of the slave system at $T=35$ from four different, closely spaced initial conditions. Two cases synchronize; the others appear never to. In fact, the second pair converges to the same solution, which is the signature of a convergence to a different attractor in the slave system. Some details of this attractor are shown in Fig. 22.

Thus although the finite-step method can potentially improve synchronization, it is flawed in its sensitivity to initial condition.

VII. CONCLUDING REMARKS

The main thrusts of this work have fallen in two directions. First, we have provided a detailed description of bifurcations along one pathway in parameter space for the Moore–Spiegel oscillator. The range of behavior that emerges is rather rich, much like the complicated tapestry woven by the Lorenz equations. Second we have studied whether identical Moore–Spiegel oscillators can synchronize in the sense of Pecora and Carroll, or through the discrete resetting of a coordinate after fixed intervals.[16]

The lesson we learn from the synchronization study is that the system as given in Eqs. (3) and (4) cannot be synchronized on using two of the coordinates, but can be with the other (x). However, even synchronization in that coordinate fails over certain parameter ranges; the determination of where synchronization is successful boils down to a numerical exercise, with few obvious clues to aid one. If one is faced with a system with given drive variables, this approach would be what one would be up against; our study will prove useful in that context.

A much more elegant approach is to recognize that by simple coordinate transformations, one can write the system in a form that is readily synchronizable. This was already known for linear coordinate transformations of systems such as Rössler's equations in some circumstances.[2] Here we have employed nonlinear changes of variable and taken the idea one step further.

In this regard, the Moore–Spiegel system proves very useful. In the process of unravelling some of the mathematical distinctions between this system, Rössler's oscillator and the Lorenz equations, Marzec and Spiegel recast all three in the form of generalized potential systems. This amounts to nonlinear coordinate transformations of the original variables, and the resulting equations can be recognized to be synchronizable (or essentially so), independently of parameter values, initial condition, and numerical experimentation. Moreover, the method is easily extended to systems of higher dimension and with more than one positive Lyapunov exponent (cf. Ref. 14).

In other words, by simply rewriting the original system, we can often engineer synchronization, a property that has

also been pointed out previously.[10] Moreover, the expression of the equations as a generalized potential system is a convenient, unifying tack to take. Put another way, we give guidelines as to exactly what combinations of coordinates one must feed into the slave from the master in order to achieve synchronization. This is an alternative to other approaches[17] that modify the equations of the slave system in order to achieve synchronization.

ACKNOWLEDGMENTS

N.J.B. thanks the Green foundation for support and R.V.C. gratefully acknowledges the financial support of an EPSRC Advanced Fellowship.

[1] L. M. Pecora and T. L. Carroll, ''Driving systems with chaotic signals,'' Phys. Rev. A **44**, 2374–2383 (1991).
[2] C. Tresser, P. A. Worfolk, and H. Bass, ''Master-slave synchronization from the point of view of global dynamics,'' Chaos **5**, 693–699 (1995).
[3] R. He and P. G. Vaidya, ''Analysis and synthesis of synchronous periodic and chaotic systems,'' Phys. Rev. A **46**, 7387–7392 (1994).
[4] D. W. Moore and E. A. Spiegel, ''A thermally excited nonlinear oscillator,'' Astrophys. J. **143**, 871–887 (1966).
[5] N. H. Baker, D. W. Moore, and E. A. Spiegel, ''A periodic behavior of a nonlinear oscillator,'' Q. J. Mech. Appl. Math. **24**, 391–422 (1971).
[6] C. J. Marzec and E. A. Spiegel, ''Ordinary differential equations with strange attractors,'' SIAM (Soc. Ind. Appl. Math.) J. Appl. Math. **38**, 403–421 (1980).
[7] C. Sparrow, *The Lorenz Equations* (Springer-Verlag, Berlin, 1982).
[8] J. Guckenheimer and P. Holmes, *Nonlinear Oscillations, Dynamical Systems, and Bifurcations of Vector Fields* (Springer-Verlag, Berlin, 1983).
[9] J. Grasman, *Asymptotic Methods for Relaxation Oscillations and Applications* (Springer-Verlag, Berlin, 1987).
[10] L. Kocarev and U. Parlitz, ''General approach for chaotic synchronization with applications to communication,'' Phys. Rev. Lett. **74**, 5028–5031 (1995).
[11] R. Artuso, E. Aurell, and P. Cvitanovic, ''Recycling of strange sets i: Cycle expansions,'' Nonlinearity **3**, 325–359 (1990).
[12] P. Cvitanovic, ''Dynamical averaging in terms of periodic orbits,'' Physica D **3**, 109–123 (1995).
[13] P. Cvitanovic and B. Eckhardt, ''Symmetry decomposition of chaotic dynamics,'' Nonlinearity **6**, 277–311 (1993).
[14] J. H. Peng, E. J. Ding, M. Ding, and W. Yang, ''Synchronizing hyperchaos with a scalar transmitted signal,'' Phys. Rev. Lett. **76**, 904–907 (1996).
[15] N. F. Rulkov, M. M. Sushchik, L. S. Tsimring, and H. Abarbanel, ''Generalized synchronization of chaos in directionally coupled chaotic systems,'' Phys. Rev. E **51**, 980–994 (1995).
[16] R. E. Amritkar and N. Gupte, ''Synchronization of chaotic orbits: the effect of a finite time step,'' Phys. Rev. E **47**, 3889–3895 (1993).
[17] R. Brown and N. F. Rulkov, ''Synchronization of chaotic systems: transverse stability of trajectories in invariant manifolds,'' Chaos **7**, 395–413 (1997).